Hyperfine Interactions 125 (2000) 113–132

Heterodyne detection of synchrotron radiation

R. Coussement, J. Odeurs, C. L'abbé * and G. Neyens **

Instituut voor Kern- en Stralingsfysica, University of Leuven, Celestijnenlaan 200 D, B-3001 Leuven, Belgium

A time integral method for the study of resonant nuclear scattering of synchrotron radiation in the forward direction is presented. The method relies on the interference of radiation scattered by nuclei in two samples, one moving with respect to the other. The method, termed heterodyne detection of synchrotron radiation, gives the same information on hyperfine parameters as the well known differential method. The general formalism is developed for the case where the reference is a single line sample and the investigated sample has magnetic or quadrupole splitting. The first experiments are discussed. A comparison of time differential synchrotron radiation spectroscopy, heterodyne detection and Mössbauer spectroscopy is given.

1. Introduction

Synchrotron radiation supplies a broad band of X-rays which is typically 10^{10}–10^{13} times energetically broader than the width Γ of most nuclear resonances. Therefore, the experimental problem when using synchrotron radiation for the detection of nuclear resonances is the selection of a narrow frequency domain out of the tremendous background of the nonresonant fraction of the incident synchrotron radiation. Until now two methods have been applied: in the first a nuclear monochromator is used to select a band $\sim 100\Gamma$, in the second the resonant radiation is separated from the nonresonant by time selection. The time selection can be performed in two modes, the time differential mode and the time integral mode. Since the first unambiguous observation [1] of synchrotron X-rays resonantly scattered by ^{57}Fe nuclei, the time differential mode was applied in many experiments in the forward scattering or in Bragg geometry (see, e.g., the reviews [2–5]). The time integral mode has been proposed recently [6] and has been given the name of heterodyne detection. The origin of the name, as explained in [7], comes from the fact that one observes the interference of a variable reference frequency with the unknown one. This idea can be used in the time differential mode as well as in the time integral mode. It is, however, only of practical use in the time integral mode.

* C. L'abbé is research assistant of FWO-Vlaanderen (Fund for Scientific Research).
** G. Neyens is post-doctoral researcher of FWO-Vlaanderen.

2. The concept

When a resonant photon interacts with one or two (or more) absorbers placed in the beam, all resonant nuclei, in whatever absorber sample they are situated, interact collectively with the photon and for each nucleus there is an excitation amplitude [8–12]. Such a collective excitation is called a "nuclear exciton" by some authors. In that sense the exciton extends to nuclei belonging to different samples. This consideration is important when we consider the collective de-excitation amplitude as a second step in the scattering process because the total scattering amplitude is the sum of all particular amplitudes A_{ij}, each associated with the photons scattered by a particular nucleus i through a particular nuclear transition j:

$$A = \sum_{i=1}^{N} \sum_{j=1}^{n} A_{ij}, \tag{2.1}$$

where N is the number of resonant nuclei participating in the process and n the number of nuclear (hyperfine) transitions that can be excited by the photon.

According to standard formulae of quantum electrodynamics, it can be shown that

$$A_{ij} = A_j \, \mathrm{e}^{-\mathrm{i}\omega_j t} \, \mathrm{e}^{\mathrm{i}(\boldsymbol{k}-\boldsymbol{k}')\cdot\boldsymbol{r}_i}. \tag{2.2}$$

$\hbar\omega_j$ is the transition energy E_j with which nucleus i at position $\boldsymbol{r}_i$ is excited, $\boldsymbol{k}$ and $\boldsymbol{k}'$ are the wave vector of an incoming and a scattered photon, respectively. A_j is a constant describing the coupling of the nucleus with the photons. The total scattering probability P is proportional to the norm squared of the total amplitude:

$$P \propto \left| \sum_{i=1}^{N} \sum_{j=1}^{n} A_{ij} \right|^2. \tag{2.3}$$

It follows immediately that the scattering probability contains cross terms, in which products of amplitudes belonging to different nuclei and different excitation energies occur:

$$\begin{aligned} P \propto N \sum_{j=1}^{n} |A_j|^2 + \sum_{j,j',j\neq j'} \mathrm{e}^{-\mathrm{i}(\omega_j-\omega_{j'})t} A_j A_{j'}^* \sum_{i,i'} \mathrm{e}^{\mathrm{i}(\boldsymbol{k}-\boldsymbol{k}')\cdot(\boldsymbol{r}_i-\boldsymbol{r}_{i'})} \\ + \sum_{j} |A_j|^2 \sum_{i,i',i\neq i'} \mathrm{e}^{\mathrm{i}(\boldsymbol{k}-\boldsymbol{k}')\cdot(\boldsymbol{r}_i-\boldsymbol{r}_{i'})}. \end{aligned} \tag{2.4}$$

The interference terms, given by the last term on the right hand side of eq. (2.4), will, however, be nonzero only if certain conditions are fulfilled. We will now explain how both energy coherence and space coherence can give rise to a nonvanishing interference term.

When the incoming photon field has a broad-band energy spectrum, like synchrotron radiation, nuclei in a hyperfine split sample can be excited to a coherent

superposition of states with different energies (energy coherence). This coherent excitation of hyperfine levels with $\omega_j \neq \omega_{j'}$ gives rise to interferences in the scattering probability. "Quantum beats" appear in the scattered radiation intensity as a function of time (see second term on the right hand side of eq. (2.4)) with beat frequencies corresponding to the energy differences of the hyperfine splittings.

The phase differences, in the interference terms, are due to the different optical path lengths travelled by the photons scattered by different nuclei:

$$\Delta\Phi_{ii'} = (\boldsymbol{k} - \boldsymbol{k}') \cdot (\boldsymbol{r}_i - \boldsymbol{r}_{i'}). \tag{2.5}$$

When a measurement is performed over an ensemble of nuclei, with the detector in an arbitrary direction, the summation over all different optical path lengths will result in a random phase integration so that the cross terms with $i \neq i'$ cancel. Only if one detects the resonantly scattered photons in some well-defined directions, more specifically the Bragg and the forward direction, nonzero interferences between different scattering amplitudes involving different nuclei occur. Indeed, in the Bragg and forward scattering directions the optical path lengths are equal or differ by a multiple of the wavelength of the scattered radiation (this is completely analogous to the familiar X-ray scattering). For these directions there is constructive interference and, as a consequence, the probability to detect, e.g., a forward scattered photon (either from a synchrotron or from a γ-source) is not simply the sum of the individual probabilities.

If two samples are used, one with a nuclear energy $\hbar\omega_1$ and another with energy $\hbar\omega_2$, in the forward scattering geometry one retains the space coherence between amplitudes from nuclei that belong to different samples (even when they are far apart in space) as the optical path lengths remain equal. If the energies in the two samples are different, e.g., because of an isomer shift, one will observe a quantum beat with a frequency proportional to the energy difference. Such quantum beats have been observed as a periodic fluctuation of the resonant forward scattered intensity. For thin samples it can be shown [12] that the intensity $I(t)$ is

$$\begin{aligned} I(t) &\propto \left| N_1 \, \mathrm{e}^{\mathrm{i}\omega_1 t} + N_2 \, \mathrm{e}^{\mathrm{i}\omega_2 t} \right|^2 \cdot \mathrm{e}^{-t/\tau} \\ &= \left(N_1^2 + N_2^2 \right) \cdot \mathrm{e}^{-t/\tau} + 2 N_1 N_2 \cdot \mathrm{e}^{-t/\tau} \cos(\omega_2 - \omega_1) t, \end{aligned} \tag{2.6}$$

where N_1 and N_2 are proportional to the number of resonant nuclei in samples 1 and 2 and τ is the lifetime of the nuclear excited state.

In time differential synchrotron radiation experiments one determines the beat frequency by studying the interference signal as a function of time. Something similar can be done by modulating the energy of the reference sample by Doppler shift. When the time average of the intensity is measured, the contribution of the interference term becomes small compared to the contribution of the first two terms of eq. (2.6), at least if the quantum beat period is short compared with the nuclear lifetime (for thin samples) or compared with the "speed-up time" (for thick samples). At some velocity, however, the two frequencies are equal and the interference term no longer depends

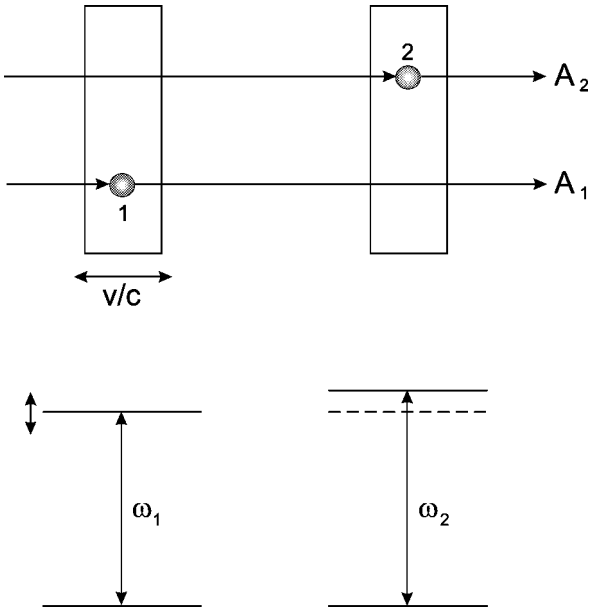

Figure 1. Visualization of scattering processes in a reference and investigated sample interacting with synchrotron radiation.

on time (except for the damping factor), so that for this velocity a maximum in the intensity is observed.

For thin samples the time average of the intensity is given by a Lorentzian:

$$I \propto N_1^2 + N_2^2 + 2N_1N_2\frac{1/\tau^2}{(\omega_2-\omega_1)^2+(1/\tau)^2}. \tag{2.7}$$

When one measures the time average of the intensity as a function of the velocity of the reference sample with respect to the investigated one, a Lorentz resonance will appear with a peak for

$$\omega_2 = \omega_1. \tag{2.8}$$

The width will be the natural width instead of two times as in Mössbauer spectrometry. The signal is positive because the interference is constructive and the signal-to-baseline ratio is given by the ratio $2N_1N_2$ to $N_1^2 + N_2^2$. When the effective thicknesses of both samples are equal, that ratio is equal to one. From the width and the signal-to-baseline ratio we see that "interference spectroscopy" and Mössbauer absorption are different.

The heterodyne method provides spectra that are due to the interference between two scattering amplitudes while the Mössbauer spectra are essentially due to the interference between one scattering amplitude and the amplitude of the direct beam [11]. This is visualized in figures 1 and 2. Notice that at resonance the scattering amplitude has a phase shift of 180° with respect to the incoming amplitude [11,12].

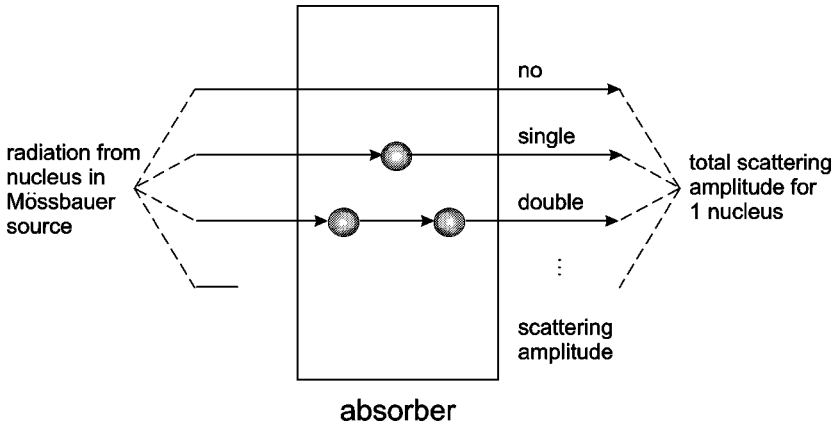

Figure 2. Schematic view of a few elementary scattering processes in a Mössbauer experiment.

Therefore, in figure 1 the two scattered amplitudes are in phase. In the case of Mössbauer absorption, figure 2, the amplitude corresponding to single scattering has a relative phase shift of 180° with respect to the amplitude corresponding to no scattering. Therefore, in the case of synchrotron radiation one has constructive interference and, consequently, interference spectroscopy. In the Mössbauer case one has destructive interference, and hence absorption spectroscopy.

The above mentioned formulae are only valid for very thin samples and do not apply to most real samples. When the samples are thick, the time evolution is no longer given by the simple formula of eq. (2.6), in which the interference term contains the product of the quantum modulation and an exponential decay function. It is now a more complex function due to the occurrence of multiple scattering [8–12]. Also the shape of the resonances in the time averaged spectra is affected by the thickness of the two samples, the reference one and the investigated one. Thickness broadening similar to that in Mössbauer spectroscopy will occur. In what follows we derive more correct formulae, using the classical "optical model" [5]. We will also include the effect of polarization of the incoming photons and of a possible orientation of the hyperfine fields in the samples.

3. Formalism

In this section the details of the theory on which the HD method is based are developed. A matrix formalism is used that describes the forward scattered radiation in the case of single line and hyperfine split samples. The reader who is not interested in the general theory, can skip this section entirely and go to section 4.

Let $E_{\mathrm{fs}}(t)$ be the γ-ray electric field corresponding to the forward scattered radiation. The time integral forward scattered intensity is given by

$$\int_0^\infty I_{\mathrm{fs}}(t)\,\mathrm{d}t = \int_0^\infty E_{\mathrm{fs}}(t)E_{\mathrm{fs}}^*(t)\,\mathrm{d}t. \tag{3.1}$$

To calculate the time average of the transmitted intensity, we will use Parseval's theorem and avoid the calculation in the time domain:

$$\int_0^\infty E_{\rm fs}(t)E_{\rm fs}^*(t)\,{\rm d}t = \frac{1}{2\pi}\int_{-\infty}^{\infty} E_{\rm fs}(\omega)E_{\rm fs}^*(\omega)\,{\rm d}\omega, \tag{3.2}$$

where $E_{\rm fs}(\omega)$ is the Fourier transform of $E_{\rm fs}(t)$.

The classical theory starts from the change in transmission amplitude through an infinitely thin sample with thickness ${\rm d}z$. It can be shown [5] that the variation of the transmitted field amplitude ${\rm d}E_{\rm tr}(z)$ after having passed through a slab of thickness ${\rm d}z$ at depth z is given by

$${\rm d}E_{\rm tr}(z) = -{\rm i}\lambda f_0 \rho E_{\rm tr}(z)\,{\rm d}z, \tag{3.3}$$

where λ is the wavelength of the radiation, ρ the concentration of resonant nuclei and f_0 the forward scattering amplitude by an individual nucleus given explicitly by (see [5])

$$f_0(\omega) = -\frac{k}{8\pi}\sigma_0\chi f_{\rm LM}\frac{\Gamma/\hbar}{\omega-\omega_0-{\rm i}\Gamma/2\hbar}. \tag{3.4}$$

k is the magnitude of the radiation wave vector, σ_0 is the maximum resonance cross section, Γ is the total width of the excited nuclear state, $f_{\rm LM}$ the recoilless fraction and χ the isotopic enrichment of the target. The solution of eq. (3.3) is simple:

$$E_{\rm tr}(z) = E_i {\rm e}^{-{\rm i}\lambda f_0 \rho z}, \tag{3.5}$$

where E_i is the (harmonic) field component of the incoming radiation with frequency ω.

Equations (3.4) and (3.5) tell us that, when a photon passes through a sample, there is a change in scattering amplitude and a change in phase. This phase shift is, of course, equivalent to the phase shift present in the quantum mechanical theories [8–12].

When photon polarization and orientation of the hyperfine field are taken into account, the scattering amplitude must receive two polarization indices σ, σ', because it depends on the polarization of the input and the output amplitude. Taking the incoming and outgoing photon direction along the z-axis, one has for a dipole transition [13]:

$$\begin{aligned} f^{\sigma,\sigma'}(\omega) = &-\frac{k}{8\pi}\sigma_0\chi f_{\rm LM}\sum_{j=1}^{n}\frac{\Gamma/\hbar}{\omega-\omega_j-{\rm i}\Gamma/2\hbar} \\ &\times C^2(j_e,1,j_g;m_e,\Delta m_j,m_g)D^{(1)}_{\Delta m_j,\sigma}(0,\theta,\phi)D^{(1)*}_{\Delta m_j,\sigma'}(0,\theta,\phi). \end{aligned} \tag{3.6}$$

The indices σ, σ', stand here for the two possible circular polarizations of the photon. σ or $\sigma' = +1$ corresponds to right circular polarization, σ or $\sigma' = -1$ to left circular polarization. The angles θ and ϕ refer to the direction of the hyperfine field with respect to the radiation axes system, which is defined with the z-axis parallel to the direction of the synchrotron radiation and with the x-axis in the plane of the linear polarization of the beam. The scattering amplitudes with $\sigma \neq \sigma'$ stand for the

Table 1
Angular dependence of the scattering amplitudes.

σ,σ'	$++$	$--$	$+-$	$-+$
$\Delta m_j = 0$	$\frac{1}{2}\sin^2\theta$	$\frac{1}{2}\sin^2\theta$	$-\frac{1}{2}\sin^2\theta\,\mathrm{e}^{-2\mathrm{i}\phi}$	$-\frac{1}{2}\sin^2\theta\,\mathrm{e}^{2\mathrm{i}\phi}$
$\Delta m_j = +1$	$\left(\frac{1+\cos\theta}{2}\right)^2$	$\left(\frac{1-\cos\theta}{2}\right)^2$	$\frac{1}{4}\sin^2\theta\,\mathrm{e}^{-2\mathrm{i}\phi}$	$\frac{1}{4}\sin^2\theta\,\mathrm{e}^{2\mathrm{i}\phi}$
$\Delta m_j = -1$	$\left(\frac{1-\cos\theta}{2}\right)^2$	$\left(\frac{1+\cos\theta}{2}\right)^2$	$\frac{1}{4}\sin^2\theta\,\mathrm{e}^{-2\mathrm{i}\phi}$	$\frac{1}{4}\sin^2\theta\,\mathrm{e}^{2\mathrm{i}\phi}$

possibility that the output amplitude has a component with a different polarization than the input amplitude. $C(j_e, 1, j_g; m_e, \Delta m_j, m_g)$ is the Clebsch–Gordan coefficient for the transition. $D^{(1)}_{\Delta m_j,\sigma}(0,\theta,\phi)$ is the matrix element describing rotations, since we allow the hyperfine field direction to be different from the forward scattering direction. The angular dependence of the scattering amplitude is contained in the product of the rotation matrix elements. The scattering amplitudes can be written more explicitly as a sum of products of a function of θ and a function of ϕ [14]:

$$f^{\sigma,\sigma'}(\omega) = \sum_j F_j(\omega, \Delta m_j) d^{(1)}_{\Delta m_j,\sigma}(\theta) d^{(1)}_{\Delta m_j,\sigma'}(\theta)\,\mathrm{e}^{-\mathrm{i}(\sigma-\sigma')\phi}, \tag{3.7}$$

where the d-functions are also defined in [14]. The expression for $F_j(\omega, \Delta m_j)$ can be found by comparing eqs. (3.7) and (3.6).

In table 1 $d^{(1)}_{\Delta m_j,\sigma}(\theta) d^{(1)}_{\Delta m_j,\sigma'}(\theta)\,\mathrm{e}^{-\mathrm{i}(\sigma-\sigma')\phi}$ is listed for different Δm_j transitions and for different polarization combinations σ, σ'. These functions will be used later when relations between the scattering amplitudes will be established for specific situations.

The differential equation (3.3) now has to be replaced by a set of two coupled linear differential equations:

$$\begin{bmatrix} \dfrac{\mathrm{d}E^+_{\mathrm{tr}}(\omega)}{\mathrm{d}z} \\ \dfrac{\mathrm{d}E^-_{\mathrm{tr}}(\omega)}{\mathrm{d}z} \end{bmatrix} = -\mathrm{i}\lambda\rho \begin{bmatrix} f^{++}(\omega) & f^{-+}(\omega) \\ f^{+-}(\omega) & f^{--}(\omega) \end{bmatrix} \begin{bmatrix} E^+_i(\omega) \\ E^-_i(\omega) \end{bmatrix}, \tag{3.8}$$

where E^+ and E^- stand for the amplitude of photons with right and left circular polarization, respectively. The nondiagonal elements of the scattering matrix are thus related to forward scattering processes in which the circular polarization changes. We will show that these nondiagonal scattering amplitudes vanish under different conditions.

For a single line absorber/scatterer we have

$$f^{\sigma,\sigma'}(\omega) = -\frac{k}{8\pi}\sigma_0\chi f_{\mathrm{LM}} \frac{\Gamma/\hbar}{\omega - \omega_0 - \mathrm{i}\Gamma/2\hbar} \sum_{\Delta m_j} \sum_{m_e} \sum_{m_g} C^2(j_e, 1, j_g; m_e, \Delta m_j, m_g) \times D^{(1)}_{\Delta m_j,\sigma}(0,\theta,\phi) D^{(1)*}_{\Delta m_j,\sigma'}(0,\theta,\phi). \tag{3.9}$$

Table 2
Relations between the scattering amplitudes for different geometries of the hyperfine field with respect to the photon beam.

General	$f^{+-} = f^{-+}\,\mathrm{e}^{-4\mathrm{i}\phi}$	
Single line	$f^{+-} = f^{-+} = 0$	$f^{++} = f^{--}$
Random orientation	$f^{+-} = f^{-+} = 0$	$f^{++} = f^{--}$
$\theta = \pi/2$		$f^{++} = f^{--}$
$\theta = 0^{*}$	$f^{+-} = f^{-+} = 0$	$f^{++} \neq f^{--}$
$\theta = 0^{**}$	$f^{+-} = f^{-+} = 0$	$f^{++} = f^{--}$

* For $\theta = 0$ only $\Delta m_j = +1$ transitions contribute to the scattering amplitude f^{++} while only $\Delta m_j = -1$ transitions contribute to f^{--}. Since for a magnetically split sample the $\Delta m_j = +1$ and the $\Delta m_j = -1$ transitions correspond to different energies (frequencies) in eq. (3.6), one has for this case $f^{++} \neq f^{--}$.

** For a quadrupole split sample, the energies corresponding to the $\Delta m_j = +1$ and the $\Delta m_j = -1$ transitions are equal, so that for this case $f^{++} = f^{--}$.

Because of the relations (see [14])

$$\sum_{m_e, m_g} C^2(j_e, 1, j_g; m_e, \Delta m_j, m_g) = 1 \tag{3.10}$$

and

$$\sum_{\Delta m_j} D^{(1)}_{\Delta m_j, \sigma}(0, \theta, \phi) D^{(1)*}_{\Delta m_j, \sigma'}(0, \theta, \phi) = \delta_{\sigma, \sigma'}, \tag{3.11}$$

one has for a single-line scatterer:

$$f^{+-} = f^{-+} = 0 \quad \text{and} \quad f^{++} = f^{--}. \tag{3.12}$$

The scattering matrix in the set of eqs. (3.8) becomes diagonal, meaning that no transfer of polarization takes place for a single-line absorber/scatterer.

If one measures over an ensemble of randomly oriented hyperfine fields, one must average over all Euler angles. From the relations (see [14])

$$\int\int D^{(1)}_{\Delta m_j, \sigma}(0, \theta, \phi) D^{(1)*}_{\Delta m_j, \sigma'}(0, \theta, \phi) \sin\theta \,\mathrm{d}\theta \,\mathrm{d}\phi = \frac{8\pi^2}{3} \delta_{\sigma, \sigma'} \tag{3.13}$$

we obtain again that the nondiagonal terms vanish and from eqs. (3.6) and (3.13) we see that $f^{++} = f^{--}$.

From examination of table 1 and eq. (3.6) one can now obtain relations between the scattering amplitudes. They are summarized in table 2.

The solution of the set of coupled linear differential equations (3.8) gives the transmitted amplitude as a function of the incoming one:

$$\begin{bmatrix} E_{\rm tr}^{+}(z,\omega) \\ E_{\rm tr}^{-}(z,\omega) \end{bmatrix} = S_{\rm I} \begin{bmatrix} E_{i}^{+}(z,\omega) \\ E_{i}^{-}(z,\omega) \end{bmatrix} \tag{3.14}$$

with $S_{\rm I}$ given by

$$\begin{aligned} S_{\rm I} &= \begin{bmatrix} A & B \\ C & D \end{bmatrix} \\ &= \begin{bmatrix} {\rm e}^{\nu z}\dfrac{\sqrt{}+a-d}{2\sqrt{}} + {\rm e}^{\mu z}\dfrac{\sqrt{}-a+d}{2\sqrt{}} & \dfrac{b}{\sqrt{}}\left({\rm e}^{\nu z}-{\rm e}^{\mu z}\right) \\ \dfrac{c}{\sqrt{}}\left({\rm e}^{\nu z}-{\rm e}^{\mu z}\right) & {\rm e}^{\nu z}\dfrac{\sqrt{}-a+d}{2\sqrt{}} + {\rm e}^{\mu z}\dfrac{\sqrt{}+a-d}{2\sqrt{}} \end{bmatrix}, \end{aligned} \tag{3.15}$$

where the symbols are defined by

$$\begin{aligned} &a = {\rm i}\lambda\rho f^{++}(\omega), \qquad b = {\rm i}\lambda\rho f^{-+}(\omega), \qquad c = {\rm i}\lambda\rho f^{+-}(\omega), \qquad d = {\rm i}\lambda\rho f^{--}(\omega), \\ &\sqrt{} = \sqrt{(a-d)^2+4bc}, \qquad \mu = \frac{-(a+d)+\sqrt{}}{2}, \qquad \nu = \frac{-(a+d)-\sqrt{}}{2}. \end{aligned} \tag{3.16}$$

To obtain the transmitted amplitude after a second absorber, the results from eq. (3.14) for the first absorber are again inserted into these equations as the new E_i, with appropriate values for a, b, c and d which are absorber dependent. The transformation of the transmitted field can be expressed by a transformation matrix $S_{\rm I}$, the matrix elements containing all parameters of the scatterer. When two different scatterers are used, the total transformation is given by the product of the two transformation matrices. The correct sequence must be respected since the two matrices do not commute in general.

For a single line scatterer or for a random distribution of hyperfine fields, we have shown that the nondiagonal scattering amplitudes are zero and the diagonal matrix elements are equal. Then the matrix becomes very simple and proportional to the unit matrix:

$$S_{\rm R} = {\rm e}^{-a_{\rm ref}d_{\rm ref}} \begin{bmatrix} 1 & 0 \\ 0 & 1 \end{bmatrix}. \tag{3.17}$$

This matrix has been called $S_{\rm R}$ (from Reference material). The symbol $d_{\rm ref}$ is used for the thickness of the reference material, $a_{\rm ref}$ is a new name for the previous symbol a.

Such a matrix commutes with any square matrix so that we can conclude that if one chooses a single-line absorber/scatterer as the reference sample, one does not have to care about the sequence of the investigated sample with respect to the reference one.

In the expressions above, the circular polarization representation of the photon is used rather than the linear polarization representation, because it is easier to express

the scattering amplitudes in the former representation. Because the SR is strongly linearly polarized and because of the polarizer/analyzer set-up, it is useful to transform from one representation to the other. The transformation from the circular to the linear representation is given by the matrix equation

$$\begin{bmatrix} E_x \\ E_y \end{bmatrix} = \frac{1}{\sqrt{2}} \begin{bmatrix} -1 & +1 \\ \mathrm{i} & \mathrm{i} \end{bmatrix} \begin{bmatrix} E^+ \\ E^- \end{bmatrix} = U \begin{bmatrix} E^+ \\ E^- \end{bmatrix}. \tag{3.18}$$

If the influence of an X polarizer and a Y analyzer is described by the matrices

$$P_x = \begin{bmatrix} 1 & 0 \\ 0 & 0 \end{bmatrix}, \qquad P_y = \begin{bmatrix} 0 & 0 \\ 0 & 1 \end{bmatrix} \tag{3.19}$$

the transmission of SR through consecutively an X polarizer, the investigated sample, the single-line reference sample and, finally, a Y analyzer, is described by the following matrix equation:

$$\begin{aligned} \begin{bmatrix} E_x^{\mathrm{out}} \\ E_y^{\mathrm{out}} \end{bmatrix} &= P_y U S_{\mathrm{R}} S_{\mathrm{I}} U^{-1} P_x \begin{bmatrix} E_x^{\mathrm{in}} \\ E_y^{\mathrm{in}} \end{bmatrix} \\ &= E_x^{\mathrm{in}} \frac{\mathrm{i}\mathrm{e}^{-a_{\mathrm{ref}} d_{\mathrm{ref}}}}{2} (-A + B - C + D) \begin{bmatrix} 0 \\ 1 \end{bmatrix}. \end{aligned} \tag{3.20}$$

When the polarizer/analyzer set-up is not used and the SR is impinging directly onto the investigated sample, one has

$$\begin{aligned} \begin{bmatrix} E_x^{\mathrm{out}} \\ E_y^{\mathrm{out}} \end{bmatrix} &= U S_{\mathrm{R}} S_{\mathrm{I}} U^{-1} \begin{bmatrix} E_x^{\mathrm{in}} \\ E_y^{\mathrm{in}} \end{bmatrix} \\ &= \frac{\mathrm{e}^{-a_{\mathrm{ref}} d_{\mathrm{ref}}}}{2} \begin{bmatrix} A - B - C + D & \mathrm{i}(A + B - C - D) \\ \mathrm{i}(-A + B - C + D) & A + B + C + D \end{bmatrix} \begin{bmatrix} E_x^{\mathrm{in}} \\ E_y^{\mathrm{in}} \end{bmatrix}. \end{aligned} \tag{3.21}$$

Equations (3.20) and (3.21) give the transformation from input amplitudes to transmitted ones, in the linear polarization base. The transformation elements are now combinations of the transformation elements in the circular polarization base (A, B, C, D). From table 2 we can deduce relations between these elements for specific cases and substitute them into eqs. (3.20) and (3.21). These relations are summarized in table 3.

Making use of these relations one can conclude that when both the reference and the investigated sample are single-line samples or have hyperfine fields that have a random orientation, no radiation is transmitted through the polarizer/analyzer set-up (eq. (3.20)). The transmission through the set-up without polarizer/analyzer is simply given by

$$\begin{bmatrix} E_x^{\mathrm{out}} \\ E_y^{\mathrm{out}} \end{bmatrix} = \mathrm{e}^{-a_{\mathrm{ref}} d_{\mathrm{ref}}}\, \mathrm{e}^{-a_{\mathrm{s}} d_{\mathrm{s}}} \begin{bmatrix} E_x^{\mathrm{in}} \\ E_y^{\mathrm{in}} \end{bmatrix}, \tag{3.22}$$

where the subscript s refers to the properties of the investigated sample.

Table 3
Relations between the elements in the transformation matrices eqs. (3.20) and (3.21) for different geometries of the hyperfine field with respect to the photon beam.

General		$C = B\,\mathrm{e}^{-4\mathrm{i}\phi}$
Single line	$A = D$	$B = C = 0$
Random orientation	$A = D$	$B = C = 0$
$\theta = \pi/2$	$A = D$	$C = B\,\mathrm{e}^{-4\mathrm{i}\phi}$
$\theta = 0$ (for magnetic splitting)	$A \neq D$	$B = C = 0$
$\theta = 0$ (for quadrupole splitting)	$A = D$	$B = C = 0$

One can draw the same conclusion for a sample that exhibits a quadrupole interaction with the electric field gradient axis parallel to the beam direction.

However, when the sample is split by a magnetic interaction with the field parallel to the beam direction, there is transmission through the polarizer/analyzer set-up, because the $\Delta m_j = +1$ and the $\Delta m_j = -1$ transitions are transmitted at different velocities of the reference sample. The transmission amplitude of $\Delta m_j = +1$ (given by A) and the amplitude of $\Delta m_j = -1$ (given by D) have opposite phase. For this reason these amplitudes cancel each other when they coincide, as in the case for quadrupole splitting.

The geometry with the hyperfine field (or electric field gradient) perpendicular to the beam ($\theta = \pi/2$) is more widely used. From eq. (3.20) one can conclude that the transmitted amplitude through the polarizer/analyzer is proportional to $B - C$ only, since $A = D$. With the relation $C = B\,\mathrm{e}^{-4\mathrm{i}\phi}$ we have $B - C = B(1 - \mathrm{e}^{-4\mathrm{i}\phi})$. This quantity depends on ϕ, the angle between the hyperfine field and the linear polarization plane of the incoming beam. For $\phi = \pi/2$, there is no transmission through the polarizer/analyzer set-up, while for $\phi = \pi/4$ there is maximum transmission.

Finally, we want to mention that the time integral forward scattered intensity is given by a modification of eq. (3.2) when two polarization components are present. One has

$$\int_0^\infty I_{\mathrm{fs}}(t)\,\mathrm{d}t = \frac{1}{2\pi}\int_{-\infty}^{\infty}\left(E_x^{\mathrm{out}}(\omega)E_x^{\mathrm{out}^*}(\omega) + E_y^{\mathrm{out}}(\omega)E_y^{\mathrm{out}^*}(\omega)\right)\mathrm{d}\omega. \tag{3.23}$$

With the aid of eqs. (3.20) and (3.21), this forward scattered intensity can thus be calculated for all geometries.

4. Experiments

4.1. Single-line samples

To test the concept of the heterodyne detection (HD) method, a first experiment was performed [15] at the APS at Argonne National Laboratory. The two samples were stainless steel foils (SS310) enriched to 42% in ^{57}Fe at room temperature, both having an effective thickness of 9. The velocity of one sample was changed sinusoidally,

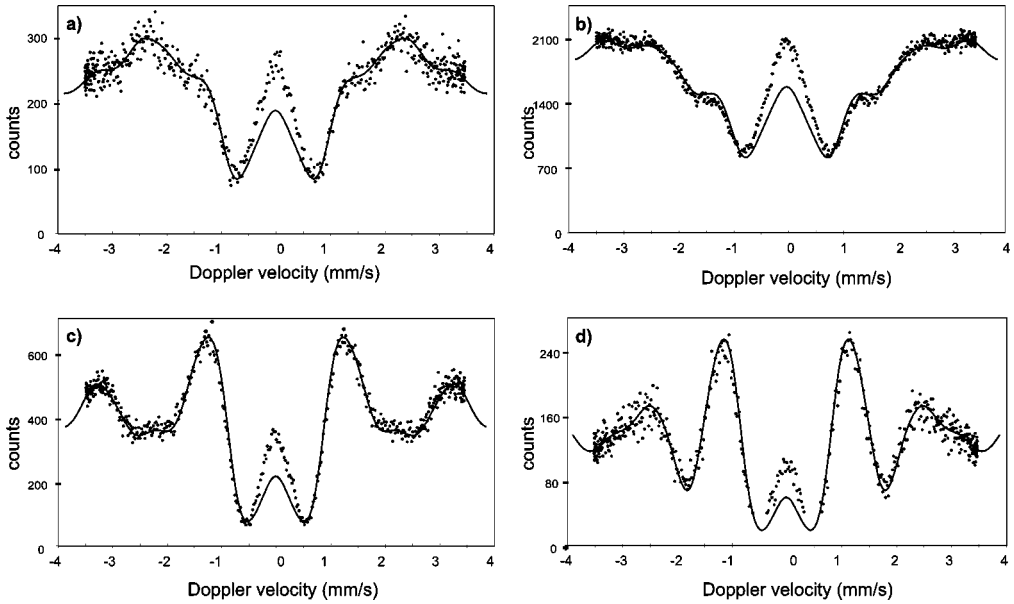

Figure 3. HD with different time windows: (a) 27.0–82.0 ns, (b) 21.5–82.0 ns, (c) 47.0–85.5 ns, (d) 58.0–85.0 ns.

while the other was kept stationary. The spectra were recorded in multichannel scaling mode (counts in the forward direction as a function of the Doppler velocity).

The high resolution monochromator was a nested 4-bounce Si crystal, consisting of an asymmetrically cut (4 2 2) channel-cut outer crystal with an asymmetry angle of -20°, and a symmetrically cut (10 6 4) channel-cut inner crystal. The energy bandpass is 5.5 meV at 14.413 keV. The synchrotron gave two pulses every 100 ns with 2.8 ns between the two pulses. They produce a prompt X-ray burst in the detector, which is followed by the delayed resonant radiation emitted from the samples. The initial X-ray burst overloads the detector to such an extent that it is "blind" during about 30 ns after the pulse. Therefore, the measurements were performed with a certain time window. Several spectra were recorded with different time windows. It is well known in Mössbauer spectroscopy that time-slicing produces some oscillations in the recorded spectrum. In the HD the oscillations are extremely sensitive to the chosen time window (figure 3). We will dwell on these oscillations in section 5.

The qualitative features of the spectra could be reproduced using a semi-classical optical model. The simulations are also given in figure 3.

There is a misfit around zero velocity, for which we do not have a satisfactory explanation at the moment. The features of the spectrum also depend strongly on the thickness of the samples. However, we would like to emphasize that the presence of the oscillations in the spectrum, due to time-slicing, complicates the interpretation, especially when several hyperfine components are present.

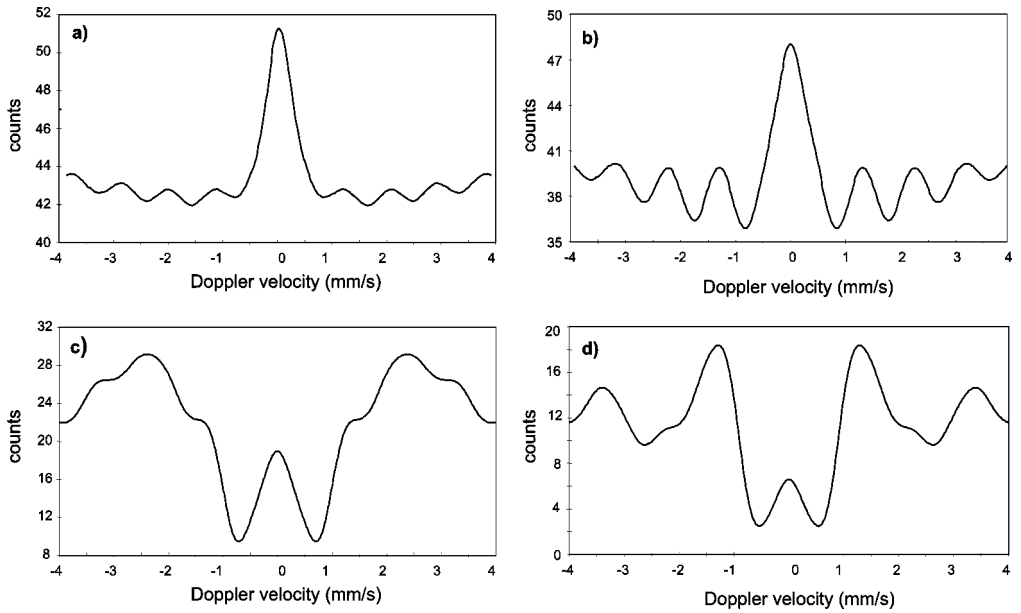

Figure 4. HD simulations for different widths of the time windows: (a) 4–99 ns, (b) 5–85 ns, (c) 25–85 ns, (d) 45–85 ns. The effective thickness of each sample is 9.

In figure 4 several simulations with different time windows are displayed for samples of ^{57}Fe having an effective thickness of 9. Generally, the oscillations are reduced if the measurements start earlier after the synchrotron pulse (compare figure 4(a) with figures 4(b)–(d)). Simulations also show that for the same time window the oscillations are somewhat less pronounced when the samples become thinner.

In the next section another measurement will be described where the direct synchrotron radiation no longer hits the detector.

4.2. Experiment with polarizer/analyzer

Here we present the result of a second experiment, performed at the same beamline, but in which we reduced the time-slicing to a minimum by using a polarizer/analyzer set-up. A schematic overview of the experiment is shown in figure 5. The undulator was tuned to the 14.413 keV nuclear resonance of ^{57}Fe. With a high-heat-load Si (1 1 1) double crystal monochromator an energy bandwidth of 3.5 eV is selected. In order to separate non-resonant from resonant radiation, we used a polarizer/analyzer pair. The investigated sample was a magnetically split Fe-foil of 2.5 μm thickness, enriched to 53% in ^{57}Fe. An external magnetic field was applied perpendicular to the SR in the plane of the foil and at 45° with respect to the polarization plane of the SR, to orient the hyperfine field. As a reference sample we used a 2.1 μm thick stainless steel foil (SS310), enriched to 95% in ^{57}Fe, which was moved. The measurement was performed with a prompt pulse distance of 100 ns. The count rate of the resonant photons was 50 s^{-1}. The resulting time integral spectrum is given in figure 6,

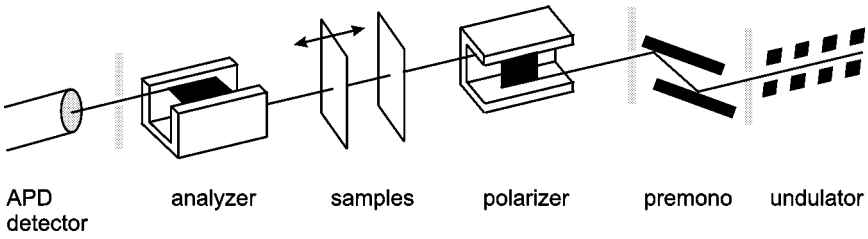

Figure 5. Experimental set-up for nuclear resonant forward scattering of synchrotron radiation. The propagation direction of the beam is from right to left.

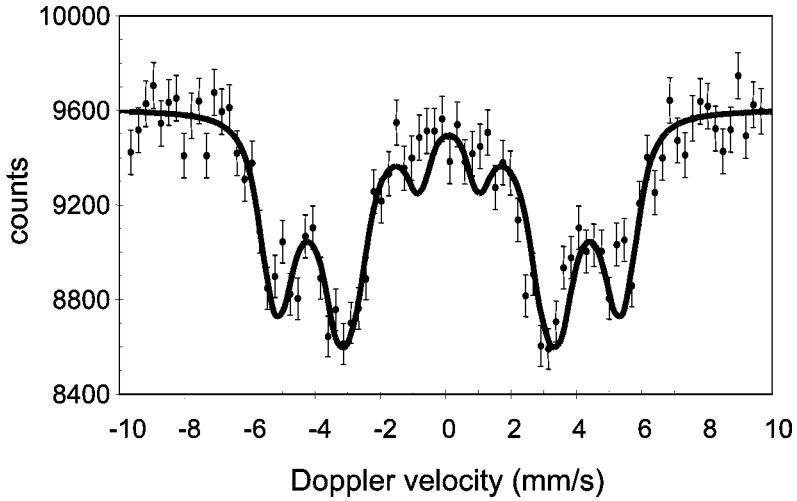

Figure 6. HD spectrum: the smooth line is a simulation.

showing the forward scattered intensity versus the velocity of the reference sample. The smooth line is a simulation based on the semi-classical theory for nuclear resonant forward scattering. The spectrum clearly shows the six ^{57}Fe peaks corresponding to transitions involving an angular momentum change $\Delta m = 0, \pm 1$. The relative intensity of the peaks is related to the degree of $\sigma \rightarrow \pi$ polarization change for that particular transition. Since the projection factors were the same for all transitions, the observed ratios were $3 : 4 : 1 : 1 : 4 : 3$.

Figure 7 gives the time differential spectrum obtained with the same investigated sample and the same magnetization at 45°, showing the forward scattered intensity as a function of time elapsed after the synchrotron pulse. It is obvious that the HD measuring technique gives more "direct" spectra which, due to their resemblance to classical Mössbauer spectra, are very easy to interpret and even allow online analysis. The HD spectrum contains the same information on the hyperfine interaction parameters as the TD spectrum, but in a more straightforward way, which makes the analysis much faster.

The main problem in this geometry was the low count rate that is inherent in the polarizer/analyzer set-up. However, if the count rate of resonant photons is 5000 s^{-1},

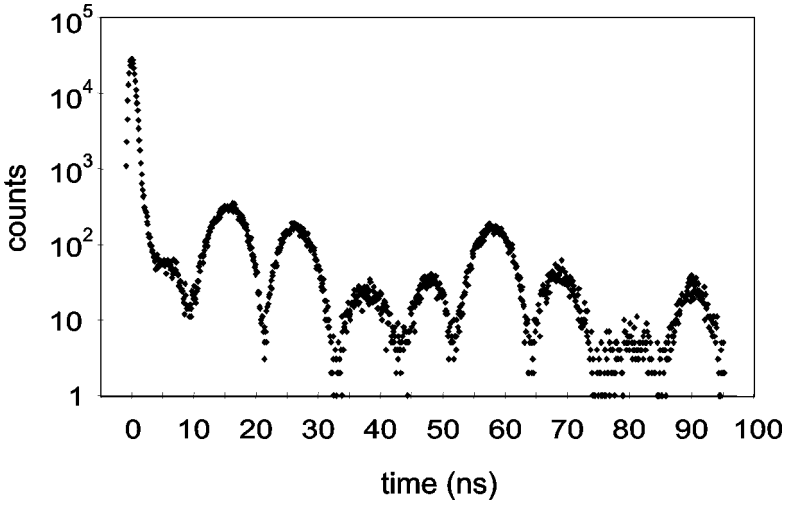

Figure 7. TD spectrum of a magnetically split Fe-foil.

the measuring time will be only a few minutes instead of several hours with the actual count rate of 50 s^{-1}. In this case the set-up with a polarizer/analyzer pair can be useful.

Another restriction of this set-up is that the investigated sample should have an oriented hyperfine field, thus excluding the study of single-line or nonpolarized powder samples. In order to optimize the HD technique and make it more generally applicable, we are still looking for alternative solutions (see section 6) to separate the nonresonant from the resonant radiation.

In the next section a brief comparison will be made between TD, HD and MS.

5. Comparison of time differential synchrotron radiation spectroscopy(TD), heterodyne detection (HD) and Mössbauer spectroscopy (MS)

The advantage of time differential spectroscopy with synchrotron radiation over normal Mössbauer spectroscopy is due to two special characteristics of a synchrotron radiation beam. The first is its sharp definition in space, i.e., the small beam cross section and the small angular divergence. This property makes synchrotron radiation very suitable for the investigation of very small samples (e.g., for high pressure studies). The second special characteristic of synchrotron radiation is its sharp definition in time, i.e., the width of the radiation pulse is of the order of 100 ps. This pulse of short duration makes synchrotron radiation highly suitable for the study of time dependent effects – stochastic or nonstochastic – with the time-differential method.

The advantages of the HD method have to be found in cases where both MS and TD are difficult. It can be used when the synchrotron is running in a timing mode that is not appropriate for the time-differential mode. This advantage is, however, limited by the fact that the detector needs some time to recover from the impact of

the synchrotron pulse. Another possible advantage will appear when one wants to study a sample with many hyperfine field components. This can be understood in the following way. In the HD method the components appear as a superposition of spectra belonging to each component while in the TD method all components interfere and the number of quantum beat frequencies can become prohibitively large in some cases.

In the HD method, one measures sequentially over the velocity range. Just as in ordinary MS, channels corresponding to the baseline yield no information on the hyperfine parameters. The fact that these channels also cost time reduces the statistical accuracy to some extent. In the TD method, this inherent loss of statistics is not present.

In TD measurements, the direct synchrotron radiation is taken away by a time-gate (the TD measurements are started about 20 ns after the synchrotron pulse), and the delayed signal comes from nuclear scattered radiation only. This would imply that the background radiation is negligible. However, the information on hyperfine interaction parameters (nuclear energy levels) is contained in the quantum beat frequencies of the TD spectra. The amplitude of the quantum beats is, according to eq. (2.6), $2N_1N_2$. The quantum beats are superimposed on a background intensity, which is $N_1^2 + N_2^2$, where the decay factor has been omitted. So the signal-to-background ratio is $2N_1N_2/(N_1^2 + N_2^2)$, as is the case for HD. The optimum for the signal-to-background ratio is in both methods obtained when the resonances of both samples have the same effective thickness. This immediately suggests a method to maximize the signal-to-baseline ratio for a particular resonance by adjusting the thickness of the reference sample to the effective thickness corresponding to the resonance of the sample. This is a particular advantage that the HD method has over Mössbauer spectroscopy.

All isotopes already studied in TD can be used in the HD method. We want to emphasize that the main reason to develop and explore the HD method is its applicability in cases where both MS and TD fail or are difficult to perform. Since the method is particularly suited for the study of long lived states, ^{181}Ta (lifetime is 8.7 μs) is a clear choice of interest. Nuclear resonant scattering of SR from ^{73}Ge (lifetime 4 μs) has not yet been observed. It would be especially interesting to add ^{73}Ge to the list, but owing to the small resonant cross section and small linewidth, it is expected that this will be very difficult.

With the polarizer/analyzer set-up the direct beam can be avoided. However, from the point of view of statistics this scheme is unfavorable compared to TD. The interference term in the HD method is a product of at least three scattering events (two in the hyperfine split sample and one in the reference sample) rather than two for the TD and consequently, the probability of these events in the HD is small compared to those of the TD. For a count rate of several kHz, the measuring time to obtain a spectrum with reasonable statistics would be a few minutes, so that HD would become practical.

A word may be said about the oscillations in the HD spectra. It is well known in Mössbauer spectroscopy [16] that time-slicing produces oscillations in the recorded spectrum. Figure 8 shows a simulated HD-spectrum for two single-line samples (^{57}Fe)

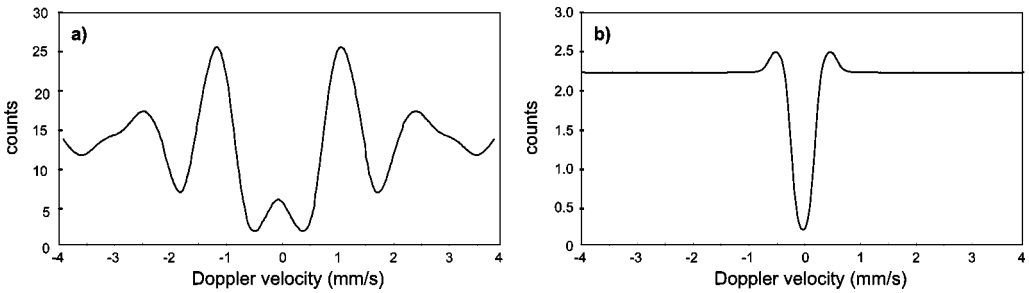

Figure 8. Simulation of a HD spectrum (a) and Mössbauer spectrum (b). Time window: 56.5–84.0 ns.

both having an effective thickness of 9, for a time window 56.5—84 ns. The same figure shows a simulated Mössbauer spectrum for a single-line source and absorber with an effective thickness of 18, for the same time window. As has been seen in section 4.1, the oscillations are much more dramatic in HD. In order to understand this different behavior due to time-slicing, a thorough numerical analysis will have to be performed. At this stage it is sufficient to mention that for SR the radiated intensity as a function of time contains a J_1 Bessel function [5], while for MS it contains the J_0 Bessel function [16], which has a different behavior [17].

Recently, Doppler absorption measurements with SR, based on the use of nuclear monochromators, have been reported. In [18], time-sliced Mössbauer absorption spectra using SR and a resonant Bragg monochromator (a mosaic crystal of $^{57}Fe_2O_3$) are given. This type of experiment is analogous to an ordinary (time-sliced) Mössbauer experiment since the input for the absorber is synchrotron radiation monochromatized to a certain degree. This explains why the oscillations are much less dramatic [16] compared to HD. In [19], Mössbauer transmission spectra are reported using single-line Mössbauer radiation extracted from broadband SR. This particular radiation was obtained by pure nuclear Bragg reflection of synchrotron radiation from a crystal of $^{57}FeBO_3$ at the Néel temperature. Here no timing was necessary and one gets in principle spectra with the same resolution as ordinary Mössbauer spectra. The HD method is different for these studies.

In the next section we will briefly outline a few (not yet realized) possibilities to reduce the effects of time-slicing.

6. Future developments

As has been mentioned, in the nuclear forward scattering mode, time differential as well as time integral, the direct beam hits the detector and makes it “blind” for a non-negligible period. The first 30 ns could not be used in the first experiments at APS in Argonne, described in section 4.1. In the TD as well as in HD one can use the polarizer/analyzer combination. However, that combination requires samples in which the hyperfine fields are oriented. This is a minor disadvantage when purely magnetic systems are studied, but requires single crystals when quadrupole interaction

is involved. Furthermore, this operational mode is statistically very inferior for HD. Therefore different concepts have to be investigated.

In a previous publication [15] we argued that the use of a nuclear monochromator could be the solution. However, a thorough analysis performed by Smirnov [20] has shown that the use of a nuclear monochromator will not be of much help in reducing the oscillations in HD. The scattering response of a thick nuclear monochromator to incident radiation is to send radiation in the Bragg direction. This scattered radiation has a fast component followed by a tail. The fast component is the important one and, according to Kagan et al. [8], the speed-up effect makes the decay occur in only a few ns for ^{57}Fe. Thus the energy bandwidth of this radiation is correspondingly large. Our intention was to use the fast Bragg component as the input signal for two samples in the HD configuration. The bandwidth of the scattered radiation should be large enough to excite the different hyperfine levels in the samples simultaneously by the radiation from the nuclear monochromator. Conventional nuclear monochromators with high electronic suppression show appreciable structure (see, e.g., the $^{57}Fe_2O_3$ nuclear (7 7 7) Bragg peak [21] or the $^{57}FeBO_3$ nuclear (1 1 1) Bragg peak [22]). Therefore, when the Bragg scattered radiation from these nuclear monochromators, is used as input for the HD, the spectrum will be complicated. In order to perform HD (as well as TD) on arbitrary samples, broadband filtering is essential, as has been explained. Two types of artificial layered structures have been proposed as nuclear monochromators: nuclear multilayers and grazing incidence antireflection (GIAR) films. GIARs are bilayer structures incorporating resonant nuclei in one of the layers. Reflection from a $^{57}Fe_5B_4C$/Ta yielded a value of 110Γ for the nuclear bandwidth [23,24]. The nuclear monochromator $^{119}SnO_2$/Pd has an energy bandpass of 123Γ [25]. Nuclear multilayers involve alternating layers of different isotopes, creating a nuclear periodicity different from the electronic diffracting periodicity. Pure nuclear Bragg reflection from [^{57}Fe(22 Å)/Sc(11 Å)/Fe(22 Å)/Sc(11 Å)] $\times$ 25 multilayers, e.g., has demonstrated that a μeV bandwidth can be produced [26,27]. Smirnov has shown [20] for a bandwidth of about 100Γ, with $5 \cdot 10^5$ counts/s of incident radiation (so that the detector problem would be solved), that the nuclear monochromator has a delayed response for about 30 ns. This delayed radiation considerably overlaps the forward scattered radiation from the samples in the HD set-up. As a consequence, the hyperfine structure of the nuclear monochromator produces a distortion of the HD spectra [20]. To reduce this distortion one would have to proceed to time-slicing again, which would introduce, as before, the other type of distortion, as shown in section 4.1 (see figures 3 and 4). One needs in fact a nuclear monochromator with a bandwidth of about 500Γ, which would correspond to a still acceptable intensity of about 10^6–$5 \cdot 10^6$ counts/s. There is, however, no concrete idea to date how to realize this.

Another possibility, proposed initially by Smirnov, would be the realization of an ultrafast shutter which would suppress the incident synchrotron radiation for a few ns. The condition for electronic Bragg reflection would be altered in such a way that the nonresonant photons are not reflected for, say, 3 ns. For instance, the interplanar distance could be changed by perturbation of the piezoelectric effect of an ultrafast

laser- or rf-pulse. For the moment this is highly speculative and a lot of research has to be done to select single crystal materials that show a sufficiently large piezoelectric effect.

Finally, one could consider the development of a string of ultra thin detectors, so that the energy of the SR beam would be divided over a large number of them. This was proposed by Baron. Each detector would then recover much faster and would count immediately after the SR-pulse.

Both TD and HD would benefit greatly from the realization of these ideas.

7. Conclusions

A novel time integral synchrotron radiation spectroscopy is presented and the results of first experiments are described. The method is based on the interference between the fields radiated by resonantly excited nuclei incorporated in two different samples. The nuclear energy of one sample is Doppler modulated with respect to the other. When the energies are equal, an extremum in the radiated intensity is observed. Maxima in the intensity occur if the simple set-up without polarizer/analyzer pair is used. In this case time-slicing had to be done because of the intensity of the nonresonant part of the incoming synchrotron pulse. The time-slicing produces oscillations in the recorded spectrum. The spectra can be simulated, at least qualitatively, by making use of the semi-classical optical model. The misfit between the simulations and the data is not yet understood. If the polarizer/analyzer set-up is used, one has minima in the transmitted intensity, each time the nuclear energy in the reference sample matches by Doppler effect that of the investigated sample. The time-slicing for this case can be reduced so that the oscillations in the recorded spectra can be minimized. However, the polarizer/analyzer set-up is unfavorable from a statistical point of view. This set-up will be useful when the count rate of resonant photons is of the order of several kHz. The major advantage of the time integral method is that it will also work in the case that the experimental timing condition, necessary for forward scattered time differential synchrotron radiation, cannot be fulfilled (long-lived isomers). Making use of new developments in the domains of detector design or ultrafast shutters, it is expected that the time-slicing can be reduced appreciably, so that the spectra will become simpler.

Acknowledgements

This work was supported by the IUAP-program P4-07, financed by the Belgian Federal Office for Scientific, Technical and Cultural Affairs, and by FWO-Vlaanderen. The authors want to thank Dr. E.E. Alp, Dr. W. Sturhahn, Dr. T. Toellner and Professor C. Johnson (APS, Argonne) for making the measurements of HD possible. Several stimulating discussions with Professor G.R. Hoy (Old Dominion University, Norfolk) are acknowledged.

References

[1] E. Gerdau, R. Rüffer, H. Winkler, W. Tolksdorf, C.P. Klages and J.P. Hannon, Phys. Rev. Lett. 54 (1985) 835.
[2] J. Arthur, E. Brown, S.L. Ruby, G.S. Brown and G.K. Shenoy, J. Appl. Phys. 67 (1990) 5704.
[3] R. Rüffer, Synchrotron Radiation News 5 (1992) 23.
[4] E. Gerdau and U van Bürck, in: *Resonant Anomalous X-ray Scattering*, eds. G. Materlik, C.J. Sparks and K. Fisher (Elsevier, Amsterdam, 1994) p. 589.
[5] G.V. Smirnov, Hyp. Interact. 97/98 (1996) 551, and many references therein.
[6] R. Coussement, S. Cottenier and C. L'abbé, Phys. Rev. B 54 (1996) 16003.
[7] R. Coussement, J. Odeurs, G. Neyens and C. L'abbé, in: *Essays on Interdisciplinary Topics in Natural Sciences Memorabilia: Jacques Danon*, eds. R.B. Scorzeli, I. Souza Azevedo and E. Baggio Saitovitch (Centro Brasileiro de Pesquisas Físicas, Rio de Janeiro, 1997) p. 55.
[8] Yu.M. Kagan, A.M. Afanas'ev and V.G. Kohn, J. Phys. C12 (1979) 615, and references therein.
[9] J.P. Hannon and G.T. Trammell, Physica B 159 (1989) 161, and references therein.
[10] J.P. Hannon and G.T. Trammell, in: *Resonant Anomalous X-ray Scattering*, eds. G. Materlik, C.J. Sparks and K. Fisher (Elsevier, Amsterdam, 1994) p. 565.
[11] G.R. Hoy, J. Phys. C 9 (1997) 8749.
[12] G.R. Hoy, J. Odeurs and R. Coussement, Quantum mechanical model for nuclear resonant forward scattering using synchrotron radiation, IKS preprint (1998).
[13] G.T. Trammell, Phys. Rev. 126 (1962) 1045.
[14] M.E. Rose, in: *Elementary Theory of Angular Momentum* (Wiley, New York, 1957).
[15] J. Odeurs, R. Coussement, C. L'abbé, G. Neyens, G.R. Hoy, E.E. Alp, W. Sturhahn, T. Toellner and C. Johnson, Hyp. Interact. 113 (1998) 455.
[16] F.J. Lynch, R.E. Holland and M. Hamermesh, Phys. Rev. 120 (1960) 513.
[17] E. Butkov, in: *Mathematical Physics* (Addison Wesley, Reading, MA, 1968).
[18] J.Z. Tischler, B.C. Larson, L.A. Boatner, E.E. Alp and T. Mooney, J. Appl. Phys. 79 (1996) 3686.
[19] G.V. Smirnov, U. van Bürck, A.I. Chumakov, A.Q.R. Baron and R. Rüffer, Phys. Rev. B 55 (1997) 5811.
[20] G. Smirnov, On heterodyne Mössbauer spectroscopy, IKS report (1998).
[21] G. Faigel, D.P. Siddons, J.B. Hastings, P.E. Haustein, J.R. Grover and L.E. Berman, Phys. Rev. Lett. 61 (1988) 2794.
[22] U. van Bürck, G.V. Smirnov, R.L. Mössbauer and Th. Hertrich, J. Phys. C 2 (1990) 3989.
[23] R. Röhlsberger, E. Gerdau, M. Harsdorff, O. Leupold, E. Lüken, J. Metge, R. Rüffer, H.D. Rüter, W. Sturhahn and E. Witthoff, Europhys. Lett. 18 (1992) 561.
[24] R. Röhlsberger, E. Gerdau, E. Lüken, H.D. Rüter, J. Metge and O. Leupold, Z. Phys. B 92 (1993) 489.
[25] E.E. Alp, T.M. Mooney, T. Toellner, W. Sturhahn, E. Witthoff, R. Röhlsberger, E. Gerdau, H. Homma and M. Kentjana, Phys. Rev. Lett. 70 (1993) 3351.
[26] A.I. Chumakov, G.V. Smirnov, S.S. Andreev, N.N. Salashchenko and S.I. Shinkarev, JETP Lett. 56 (1992) 509.
[27] A.I. Chumakov, G.V. Smirnov, A.Q.R. Baron, J. Arthur, D.E. Brown, S.L. Ruby, G.S. Brown and N.N. Salashchenko. Phys. Rev. Lett. 71 (1993) 2489.